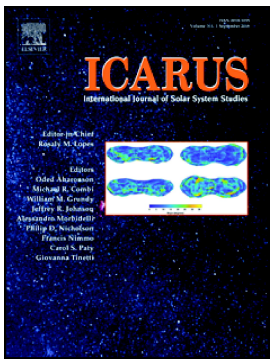

Santorini volcano as a potential Martian analogue: The Balos Cove Basalts

A. Pantazidis, I. Baziotis, A. Solomonidou, E. Manoutsoglou, D. Palles, E. Kamitsos, A. Karageorgis, G. Profitiliotis, M. Kondoyanni, S. Klemme, J. Berndt, D. Ming, P. Asimow

PII: S0019-1035(18)30681-X
DOI: https://doi.org/10.1016/j.icarus.2019.02.026
Reference: YICAR 13211

To appear in: *Icarus*

Received date: 31 October 2018
Revised date: 18 February 2019
Accepted date: 22 February 2019

Please cite this article as: A. Pantazidis, I. Baziotis, A. Solomonidou, et al., Santorini volcano as a potential Martian analogue: The Balos Cove Basalts, Icarus, https://doi.org/10.1016/j.icarus.2019.02.026

Santorini volcano as a potential Martian Analogue: the Balos Cove Basalts

Pantazidis, A.[1], Baziotis, I. [1], Solomonidou, A.[2,3], Manoutsoglou, E.[4], Palles, D.[5], Kamitsos, E.[5], Karageorgis, A.[6], Profitiliotis, G.[7], Kondoyanni, M. [1], Klemme, S.[8], Berndt, J.[8], Ming, D.[9], Asimow, P.[10]

[1]Agricultural University of Athens, Mineral Resources and Agricultural Engineering, Iera Odos str. 75, 11855 Athens, Greece, [2]European Space Agency (ESA), European Space Astronomy Centre (ESAC), Madrid, Spain. [3]LESIA-Observatoire de Paris, Paris Sciences and Letters Research University, CNRS, Sorbonne Université, Université Paris-Diderot, Meudon, France, [4]Technical University of Crete, Greece, [5]National Hellenic Research Foundation, Athens, Greece, [6]Hellenic Centre for Marine Research (HCMR), Institute of Oceanography, Athens, Greece, [7]National Technical University of Athens, [8]Westfälische Wilhelms-Univ. Münster, Institut für Mineralogie, Correnstrasse 24, Münster, Germany, [9]NASA Johnson Space Center, Houston, Texas 77058, U.S.A., [10]California Institute of Technology, Geological and Planetary Sciences, Pasadena, California, USA

*Corresponding author. Telephone: +30-2105294155. E-mail: ibaziotis@aua.gr

Abstract

The interpretation of geologic processes on Mars from sparse meteorite, remote sensing and rover data is influenced by knowledge gained from well-characterized terrestrial analogues. This calls for detailed study of candidate terrestrial analogues and comparison of their observable features to those encountered on the surface of Mars. We evaluated the mineralogical, geochemical, and physical properties of the Balos cove basalts (BCB) from the island of Santorini and compared them to Martian meteorites, Mars rover surface measurements, and other verified Martian analogues obtained from the International Space Analogue Rockstore (ISAR). Twenty rock samples were collected from the Balos cove area based on their freshness, integrity, and basaltic appearance in the field. Optical microscopy of BCB revealed a pilotaxitic to trachytic texture, with olivine and clinopyroxene phenocrysts in a fine groundmass of olivine, clinopyroxene, plagioclase, magnetite, and devitrified glass. All major minerals show normal zoning, including calcic plagioclase (An_{78-85} at the core and An_{60-76} at the rim), augite ($En_{36-48}Wo_{41-44}Fs_{11-21}$), and olivine ($Fo_{74-88}$). The dominant bands in the infrared-attenuated total reflectance (IR-ATR) spectra from BCB can be assigned to olivine (~875 cm^{-1}), calcic plagioclase (~1130 cm^{-1}), and augite (~970 cm^{-1}). The whole-rock chemical compositions and mineralogy of the BCB are similar to published analyses of typical olivine-phyric shergottites and basalts and basaltic materials analyzed in Gusev and Gale craters on Mars. BCB porosity is in the range of 7-15 % and is similar to the porosities of the ISAR samples. Although no terrestrial rock is ever a perfect match to Martian compositions, the differences in mineralogy and geochemistry between BCB and some classes of Martian samples are relatively subtle and the basalts of Santorini are as close a match as other accepted Mars basalt analogues. The Santorini site offers excellent field logistics that, together with the petrology of the outcrop, makes it a valuable locality for testing and calibration deployments, field training, and other activities related to current and future Mars exploration.

Keywords: comparative planetology; basalts; Martian analogues; mineral chemistry; planetary geology; Santorini volcano

1. Introduction

Our understanding of the Earth's interior has developed over many years as practitioners of geophysics, geodesy, geochemistry, petrology, and other disciplines have gathered and shared their observations. Our corresponding level of understanding of Mars' interior, however, is still in a primitive stage. Landed missions to the surface have provided geochemical and mineralogical information of surface basalts, but only at a handful of sites on the surface (Ares Vallis, Gusev crater, Meridiani Planum, Gale crater) (e.g., Rieder et al., 1997; Ming et al., 2008; McSween et al., 2009; Reider et al., 2004; Morrison et al., 2018). The NASA InSight mission to Mars, with an advanced seismometer (Seismic Experiment for Interior Structure-SEIS) and geothermal probe (Heat Flow and Physical Properties Probe-HP^3), has landed on Mars (late 2018 landing) and will provide the first geophysical measurements from the surface in 2019. Unlike the Moon, sampled by the Apollo and Luna missions for detailed study on Earth (Neukum and Ivanov 1994), no samples have been returned from the surface of Mars.

In the absence of returned samples, Martian meteorites (e.g., Treiman et al., 2000) and terrestrial analogues (e.g., Marlow et al., 2008) have been used to develop a framework for interpretation of data from Mars and characterization of its geologic evolution. The Martian meteorite population (formerly called the shergottite-nakhlite-chassignite (SNC) group; McSween, 2015) is dominated by shergottites. Due to that, we focus on that subset of meteorites in the current study. The predominant minerals in shergottites are clinopyroxene (Cpx), plagioclase (Pl; generally shock-amorphized to maskelynite), olivine (Ol) and spinel (Stolper and McSween, 1979; Goodrich, 2003). Nakhlites and chassignites are cumulates of augite and olivine, respectively,

Arid and basaltic terrestrial regions (e.g., Mt. Etna, Italy; the Barberton region, South Africa; Tenerife, Canary Islands; Svalbard, Norway; Mauna Kea, Hawaii) have been promoted as Mars analogues on the basis of similarities in geochemical, spectral, and mineralogical and environmental (?) characteristics (e.g., Moroz, 1978; Snook and Mendell, 2004; Morris et al., 2000). Not only do analogue samples aid in directly understanding Martian samples, they also play an important role as calibration standards for instruments slated for Mars surface operations (e.g., Bell et al., 2003). Recognizing the need for analogue samples, the National Center of Scientific

Research in Orleans (France) created the International Space Analogue Rockstore (ISAR) as a repository and database of terrestrial samples characterized as Martian analogues (Bost et al., 2013). Extending the currently available Martian rock analogue (rocks with properties similar to martian rocks and/or soils) database with additional sites and samples will enhance the diversity and utility of the repository and promote the geologic interpretation of similar materials on the surface of Mars.

We focus on an outcrop on the southern part of the Santorini volcano (Balos cove, 36°21.7'N, 25°23.8'E), one of the few basaltic localities in the South Aegean arc (Greece). This area consists of scoria and pyroclastic rocks with a composition ranging from basalt to andesite. We applied a range of complementary techniques to evaluate the chemical, mineralogical, physical, petrological, and spectroscopic properties of the Santorini basalts. The primary goal was to compare these properties with those of shergottites, and to surface igneous rocks characterized by landers on the Martian surface (meteorites and surface compositions). Secondly, we present comparisons of the Santorini results to other analogue samples from the ISAR.

2. Geological setting

The Santorini volcano (Fig. 1a) is located 110 km north of the island of Crete, lying 150 km above the Wadati-Benioff zone of the Aegean arc, where the African plate subducts northward beneath the Eurasian continent (Papazachos et al., 2000). The Santorini area is the most active within the South Aegean volcanic arc (Fig. 1b) and incorporates a group of islands namely Thera, Thirasia, Aspronisi, Palea, and Nea Kameni. These islands of the Santorini group are remnants of a former stratocone (Reck, 1936). They form a ring, enclosing a large (11×7 km) submarine caldera, inside which lie the central islands of Nea Kameni and Palaia Kameni (Nicholls, 1971).

The volcanic history of Santorini began at about 650 ka with the oldest eruptive centers located on the Akrotiri Peninsula and in the north part (Peristeria volcano) of the island (Druitt et al., 1999; Fig. 1a). These older eruptive products are overlain by the pyroclastic deposits from twelve major Plinian and several interplinian explosive eruptions (Ferrara et al., 1980), which ranged in composition from rhyolitic to andesitic and calc-andesitic. Until about 550 ka, the volcano erupted small volumes of basaltic to rhyodacite composition material. At 360 ka the activity became more

explosive with at least four caldera collapse events (Heiken and McCoy, 1984). Since the major Plinian historic Minoan eruption at 3.6 ka, an intracaldera edifice of about 3 km^3 has developed the islands of Palea Kameni and Nea Kameni (Parks et al., 2012).

The rocks on Santorini are grouped into four different series based on their field relationships and petrographic and chemical characteristics (Nicholls 1970): (a) the lavas and cognate materials of the Lumaravi-Archangelo Series, (b) the lavas and cognate materials of the Akrotiri-Thera Series, (c) the "main" Series, lavas and dykes from Peristeria, Simandiri and Skaros-Thirasia volcanoes, and (d) the modern lavas and cognate xenoliths of the historic volcano. Each of the aforementioned series, all calk-alkaline in character, display a wide compositional range from basaltic to rhyodacite (Huijsmans, 1985; Huijsmans et al., 1988).

Balos cove basalts

The Balos cove area exposes pyroclastic deposits of the first eruptive cycle of the Akrotiri-Thera series (650-550 Ka) (Nicholls, 1971; Druitt et al., 1999) (Fig. 1c). Previous maps indicate a limited compositional range in the Balos area, from basalt to andesite (Nicholls, 1971). Previous descriptions of the basalts in the area (Andújar et al., 2015) report crystal fractions near ~40 vol% in vesicular glass or groundmass, divided into ~7 vol% macrophenocrysts of Fo_{74-78} olivine (~500 μm in diameter), ~32 vol% microphenocrysts (up to ~50 μm in length) of plagioclase (An_{78-80} at the core and An_{72} at the rim), and ~2 vol% clinopyroxene (70-100 μm in length). Hence, the BCB samples may be described as olivine-phyric basalts. Microcrysts (<30-50 μm in diameter) of olivine, plagioclase, clinopyroxene, magnetite, and ilmenite also occur in the groundmass. Andújar et al., 2015 reported orthopyroxene microcrysts, but we did not observe them in our thin sections.

3. Material and Methods

We collected 20 rock samples based on their freshness, integrity, and basaltic appearance in the field. From this collection, the least weathered basalts, according to a preliminary study, were selected for detailed characterization (see also Baziotis et al. 2018). We used a range of techniques to characterize their porosity, mineralogy, geochemistry, and spectroscopic properties. We also characterized samples obtained from the ISAR, including a thin section of a Gusev basalt analogue (thin section 09SJ15-1, Bost et al., 2013), two basalt fragments (09SJ15, Svalbard, Norway;

05IS01, Lambahraun, Elborgir, Iceland), and four basalt powders (09SJ15, Svalbard, Norway; 05IS01, Lambahraun, Elborgir, Iceland; 05IS03, Bjarnalón, Hekla, Iceland; 07ZA20-1, Komati river, Barberton, South Africa). Sample 09SJ15 is proposed as an analogue for the alkali-rich tephritic Gusev class basalts encountered by the Spirit rover in Gusev crater (Bost et al., 2013). Samples 05IS01-03 and 07ZA20-1 are analogs for Noachian basalts (Bost et al., 2013). Although data for sample 09SJ15 are published in Bost et al. (2013), we re-analyzed this section in order to obtain an internally consistent database for BCB and ISAR rocks and avoid inter-laboratory bias (we also have unpublished analyses of the Tissint olivine-phyric shergottite from our microprobe that are consistent with published values from other laboratories). Basic information for each of the analyzed samples (BCB and ISAR) is given in Table 1.

3.1 Mineralogical Properties

Polished thin sections were prepared for nine selected Balos cove basalt rock fragments and one ISAR sample (09SJ15). Polarized transmitted and reflected light microscopy were used to identify phenocryst and matrix minerals. In addition, we used backscattered electron images obtained with a JEOL JSM 5600 scanning electron microscope to characterize rock textures.

3.2 Mineral Chemistry

Mineral chemistry was characterized with a JEOL JXA-8530F (University of Muenster) electron probe microanalyzer (EPMA) equipped with five wavelength-dispersive spectrometers (WDS) and one Energy Dispersive Spectrometer (EDS) and a JEOL JXA-8900 Superprobe (Agricultural University of Athens) equipped with four WDS and one EDS. All analyses used 15 kV accelerating voltage, 15 nA beam current, 1-2 μm focused beam, 20 s on-peak counting time and 10 s for each background. Smithsonian Microbeam Standards (obtained from the Department of Mineral Sciences of the Smithsonian Institution) were used as calibration standards and included albite (Al), quartz (Si), jadeite (Na), rutile (Ti), almandine (Fe), olivine (Mg), diopside (Ca), microcline (K), apatite (P), chromite (Cr), and Ni-oxide (Ni). The chemical analyses are given in Tables 2 and 3.

3.3 Bulk Properties

Whole-rock major and trace element concentrations were determined on fused beads, and pellets of pressed rock powder, respectively, using the X-ray fluorescence (XRF) wavelength spectrometer (Panalytical PW-2400) of the accredited according to ELOT EN ISO/IEC 17025:2005 biogeochemical laboratory of the Hellenic Centre for Marine Research. Major elements were determined as oxides following the procedure described in Karageorgis et al. (2005). For trace element determination, X-ray counts were converted to concentrations using the Panalytical Axios ProTrace standards and protocol, which includes 500 ppm and 1000 ppm concentration standards (n=25) for each of 40 elements, calibrated against more than 200 international reference materials. The analytical precision is 5–10% on the basis of duplicate runs of standards and unknowns. Accuracy was assessed using the secondary geological standard PACS-2, for those elements included in the protocol and also assigned a standard reference value in PACS-2. Reported detection limits are based on count rates and background statistics. Recent participation in a blind interlaboratory exercise organized by the International Atomic Energy Agency revealed optimal performance of the XRF system and applications for the determination of major and trace elements (Table 3 in IAEA, 2013; laboratory code No. 11). Whole-rock chemistry results, reference and measured values of the PACS-2 standard, and detection limits are given in Karageorgis et al. (2005). The whole-rock data are given in Table 4.

Bulk rock mineralogy was determined by X-ray Diffraction Analysis (XRD) on powdered samples using a Siemens Diffractometer D-5000 equipped with Cu Kα radiation (λ = 1.54184 Å) and Ni filter. The instrument was run at 35 kV and 25 mA. Patterns were collected at room temperature (25 °C) from 2θ = 3° to 70° at a scan speed of 0.02 °/s and 0.02° step size.

3.4 Spectroscopic Properties

The spectroscopic properties were identified using the *Fourier-transform infrared spectroscopy (FTIR) - Attenuated total reflectance (ATR)* method at the Institute of Theoretical and Physical Chemistry of the National Institute of Research (Athens, Greece). The Equinox 55 instrument was equipped with a single diffraction diamond and a mechanically rotating press. Each IR-ATR spectrum represents an average of hundreds of "strikes" in the range of 525-2500 cm^{-1} and a resolution of 4 cm^{-1}. Band

assignments of our data were based on comparison to reference mineral spectra from the RRUFF database (Lafuente et al., 2015).

3.5 Physical Properties

Texture and porosity were measured on polished thin sections using two-dimensional analysis in ImageJ/Phase Quant software. The threshold value for open voids in a mosaic of high-resolution backscattered electron was measured and applied to determine the porosity. The details of the method are described in the software tutorial (Schneider et al., 2004) and in Buckman et al. (2017).

4. Results

4.1 Mineral and Textural Properties

The BCB are characterized by fragmented euhedral olivine (Ol) and euhedral to subhedral pyroxene (Cpx) phenocrysts (<600 μm diameter) (Figs. 2 and 3). The groundmass includes smaller crystals of Ol and Cpx (~100 μm in diameter) but is dominated by prismatic or skeletal crystals of un-twinned plagioclase (Pl) (100 – 200 μm long axes) with, in many cases, a strong shape-preferred orientation (Figs. 2 and 3). The BCB exhibit textures from pilotaxitic to trachytic depending on the degree of preferred orientation of tabular Pl. Scarce quartz crystals occur as xenocrysts. Magnetite is present in the groundmass. Porosity estimates range from 7-15 vol%.

ISAR sample 09SJ15 contains subhedral phenocrysts of olivine (Fig. 4a,b) in a groundmass of prismatic plagioclase (<100 μm in diameter), pyroxenes and glass. Quartz occurs as xenocrysts (Fig. 4c,d). The texture is porphyritic. Reddening of materials around vesicles and pores suggest Fe oxidation. The porosity ranges up to 20 vol%.

4.2 Mineral Chemistry in Selected BCB and ISAR Samples

4.2.1 *Olivine*

BCB olivine has a forsterite (Fo) content ranging from Fo_{66} to Fo_{86} (Fig. 5, Table 2). In samples Bal-2 and Bal-4A, olivine is unzoned and strictly Mg-rich (Fo_{86-82}). Olivine in Bal-4B is a bit more Fe-rich, with Fo_{77-83}, while several crystals are zoned (Fo_{85} in the core and Fo_{74} in the rim). Olivine in Bal-5 is strongly zoned, with Fo_{80-84} in the core and Fo_{75-66} in the rim.

Olivine in ISAR 09SJ15 sample has a restricted crystal-to-crystal variation, with a total range Fo_{80-91} (Fig. 5, Table 3).

4.2.2 Plagioclase

Crystal-to-crystal variations in plagioclase composition in sample Bal-4A extend over a substantial range,An_{66-85}. In contrast, Bal-4B plagioclase exhibits a more restricted range, An_{66-78}. Plagioclase compositions in Bal-2 and Bal-5 have anorthite up to An_{80}, very close to the composition observed in Bal-4B (Fig. 5).

The plagioclase composition in ISAR 09SJ15 is in the range of An_{38} to An_{56} (Fig. 5, Table 3).

4.2.3 Pyroxenes

BCB pyroxenes plot within the fields of augite and diopside on the En-Fs-Wo ternary diagram (Fig. 5). Bal-4A pyroxene is in the range $En_{38-51}Wo_{48-33}Fs_{14-16}$ and Bal-4B pyroxene ranges from $En_{44}Wo_{42}Fe_{13}$ to $En_{52}Wo_{32}Fs_{16}$. Bal-5 pyroxene ranges from $En_{47}Wo_{37}Fs_{20}$ to $En_{41}Wo_{38}Fs_{12}$. Bal-2 pyroxene varies from $En_{45}Wo_{33}Fs_{12}$ to $En_{51}Wo_{37}Fs_{12}$ (Table 2).

Pyroxene in ISAR 09SJ15 is augite with a compositional range from $En_{32}Wo_{48}Fs_{20}$ to $En_{41}Wo_{47}Fs_{13}$ (Fig. 5, Table 3).

4.3 Bulk Properties

4.3.1 Whole-Rock Chemistry

X-ray fluorescence oxide chemistry on BCB samples show a narrow range for most major elements: SiO_2 is in the range of 49-51.2 wt%; CaO, 10.6-11.1 wt%; FeO*, 8.3-9.1 wt%; MgO, 5.9-6.4 wt%; and Na_2O, 2.0-2.2 wt% (Table 4). Minor elements are also fairly homogeneous: P_2O_5, 0.08-0.1 wt%; MnO, 0.15-0.16 wt%; and K_2O, 0.37-0.53 wt% (Table 4). The BCB samples plot in the basaltic region on the Total Alkali Silica (TAS) diagram (Fig. 6).

4.3.2 Modal Mineralogy

Mineral abundances based on powder X-ray diffraction for selected BCB (Bal-2, Bal-3, Bal-4A, Bal-4B, Bal-5, Bal-6, Bal-7, Bal-8) and ISAR (09SJ15, 05IS02, 05IS03, and 07ZA20-1) samples are shown in Table 1.

The BCB samples are fresh, with dominant forsteritic olivine, plagioclase and clinopyroxene and no detected alteration phases, including no X-ray amorphous features (i.e., broad diffraction "hump"). Plagioclase diffraction peak positions indicate intermediate composition in all samples except Bal-4A, which is closer to anorthite (Table 2).

Olivine, plagioclase, and quartz are present in the ISAR analogue sample 05IS02. Dominant minerals in ISAR 05IS03 are intermediate plagioclase and clinopyroxene. Olivine, intermediate plagioclase, clinopyroxene, and illite are the dominant minerals in analogue sample ISAR 09SJ15. Sample ISAR 07ZA20-1 shows dominantly plagioclase (mainly anorthite), clinopyroxene, amphibole and quartz (Table 3). The presence of illite and amphibole in 09SJ15 and 07ZA20-1 suggests that these samples have experienced aqueous alteration after formation by igneous processes.

4.4 Spectroscopic Properties

The BCB and ISAR samples display similar characteristic bands in IR-ATR spectra (Fig. 7a-d). In particular, the bands at ~875, 1130 and 970 cm^{-1}, are readily assigned to Ol, calcic Pl and augite, respectively (Table 5).

5. Discussion

5.1 Comparison of BCB with ISAR samples

Olivine in BCB is more Fe-rich than those analyzed in ISAR sample 09SJ15. In addition, the BCB pyroxene and plagioclase are generally more Ca-rich than in ISAR sample 09SJ15 (Tables 2, 3). Paradoxically, the olivine compositions suggest that the BCB samples are more fractionated than the ISAR sample, whereas the pyroxene and especially the plagioclase suggest the opposite.

The whole-rock major element compositions of the BCB samples all plot in the basalt region on the TAS diagram (Fig. 6), whereas the various ISAR samples plot in various regions on the TAS diagram. In particular, ISAR 07AZ20 plots very close to the tephrite-picrite boundary, 09SJ15 plots in the tephrite field, and 05IS01 overlaps with BCB in the basalt field.

XRD analyses indicate that BCB samples are unweathered, with detection only of primary igneous minerals. In contrast, the mineralogy of the ISAR samples varies

among sampling localities. Some are olivine-free (05IS03, 07ZA20-1) and others olivine-bearing (05IS02, 09SJ15). One sample (09SJ15) shows a clear signature of aqueous alteration by the presence of illite. The XRD peak positions for plagioclase in the various samples are consistent with the electron probe data showing that plagioclase in BCB is more calcic than in the one ISAR sample studied. In fact, all the ISAR samples exhibit XRD peak positions for plagioclase consistent with more intermediate compositions than the BCB samples.

5.2 Comparison of BCB with Martian compositions

The whole-rock chemistry of BCB can be compared with the Adirondack, Irvine, Backstay and Algonquin Class rocks in Gusev crater (data from Ming et al., 2008) on a TAS diagram (Fig. 6). We also plot the compositions of the Bounce Rock obtained by the Opportunity rover at Meridiani Planum (Zipfel et al., 2011). BCB and Gusev crater basalts have similar total alkali concentrations but they differ in their silica content. Adirondack class basalts, in particular, plot in the picrobasalt field due to low SiO_2 contents but have the closest overall composition to the BCB samples of all martian surface rocks. Furthermore, the average composition of the Martian surface basalts are Fe-rich and Al-poor compared to all the terrestrial basalts considered in this study (Fig. 8).

With respect to Martian meteorites, although quite a number have been recognized (214 as of 8th October 2018), only 23 of these are olivine-phyric shergottites (Meteoritical Bulletin database). Olivine-phyric shergottites (Goodrich, 2002) are a subtype of basalts with porphyritic olivine textures (e.g., Stolper and McSween, 1979; Rubin et al., 2000; Goodrich, 2003; Greshake et al., 2004). This population is sufficient, however, to demonstrate that the BCB olivine-phyric basalt compositions are coincident with the alkali-rich subset of the basaltic and olivine-phyric shergottites (Martian Meteorites Compendium https://curator.jsc.nasa.gov/antmet/mmc/).

The modal mineralogy of Gusev basalts (McSween et al., 2008) determined from joint modeling of Mossbauer spectra (for Fe-bearing minerals) and Alpha particle X-ray spectrometer (APXS) compositional analyses from the Spirit rover is interpreted to range from 6-23 vol% olivine, 17-47 vol% pyroxene, and 35-56 vol% plagioclase. BCBs have a similar range of modal mineralogies, with 10-12 vol% olivine, 10-15% vol% clinopyroxene and 45-50 vol% plagioclase. The proportion of olivine in the

olivine-phyric shergottites (20-29 vol%; McSween et al., 2004, 2006a,b) is somewhat higher than in typical Gusev basalts or in the BCB samples.

The olivine phenocrysts of olivine-phyric shergottites are strongly zoned with magnesian cores and ferroan rims. Due to the lack of appropriate rover instrumentation, it is not known whether the Gusev basalt olivines are zoned (McSween et al., 2006), and it is difficult to compare the wide range of spatially-resolved olivine analyses from shergottites (Fo_{84-25}) with the unresolved average values from Spirit rover data (Fo_{60-40}; Morris et al., 2004; McSween et al., 2004). The EPMA analysis in BCB showed that the large olivine grains are zoned from Fo_{79-81} in the core to Fo_{71} at the rims and the contact with groundmass; this is weaker zoning than in many shergottites, but it is not clear how it compares to any zoning that might be present in Gusev basalts.

Olivine in BCB has a higher forsterite content than is typical of the olivine-phyric shergottites, but is similar to olivine in basaltic shergottites (Fig. 5). BCB pyroxene partly overlaps pyroxene compositions in olivine-phyric shergottites. The plagioclase composition in BCB is Ca-rich compared to that in olivine-phyric shergottites. However, the Dag 476 and Dhofar 019 meteorites host plagioclase with almost identical compositions to BCB samples Bal-2, Bal-4b, and Bal-5.

We therefore conclude that, chemically and mineralogically, the BCB show sufficient similarities to Gusev crater basalts and olivine-phyric shergottites to be strongly considered as Mars basalt analogues.

5.3 Balos cove basalts as a viable analogue

Basalts exposed at the Earth's surface undergo various degrees of alteration (or weathering) depending on environmental conditions, duration of exposure to those conditions, and rock porosity. Several of the ISAR samples have mineralogy (i.e., illite) suggesting exposure to aqueous alteration. The BCB basalts are comparatively "fresh" and unaltered compared to the ISAR samples included in this study and to many other terrestrial basalts. No secondary alteration products including X-ray amorphous materials were observed in the BCB samples, contributing to its value as an analogue for relatively unaltered Martian basalts such as the Adirondack class basalts in Gusev crater.

There are, however, chemical differences between the BCB and Martian basalts. Nearly all terrestrial basalts (including BCB and ISAR rocks) are enriched in Al and depleted in Fe compared to Martian surface basalts (see figure 8 and Supplementary Figures S1-S9, where the Martian surface and meteorite samples and BCB are compared to density distributions of the GEOROC and PETDB collections of terrestrial basalt analyses). The Fe-rich character of the latter is interpreted to be related to FeO-enrichment of the Martian mantle, compared to the terrestrial mantle (e.g., Dreibus and Wänke, 1985). The Al-poor character of Martian basalts is reflected in comparatively low modal plagioclase abundance compared to terrestrial basalts and is also thought to reflect a global difference in mantle source composition compared to the Earth, perhaps as the result of the formation of a magma ocean (Bridges and Warren 2006). These bulk chemical differences are a major limitation for matching Martian surface compositions with any terrestrial analogue.

However, a strong case can be made for the inclusion of BCB as an analogue material for Mars surface basalts based on similarities in modal mineralogy and mineral chemistry. BCB olivine, pyroxene, and plagioclase modal mineralogies are all similar to their igneous counterparts on Mars based upon normative mineralogy (McSween et al., 2009) as described above. Recently, Morrison et al. (2018) have provided mineral chemistries for olivine, pyroxene, and plagioclase in Gale crater based upon the refinement of their unit cell parameters. Unit cell parameters were refined from the X-ray diffraction data derived from the Chemistry and Mineralogy (CheMin) instrument onboard the Curiosity rover in Gale crater. Although the samples analyzed in Gale crater by CheMin discussed here are unconsolidated sand/soil and sedimentary rock, they are almost certainly contain detrital minerals formed by igneous processes in the Gale crater region. Clinopyroxene (high-Ca) compositions, determined in only three out of 13 samples from Gale crater, are similar to those from BCB (Fig. 5). In particular, Gale crater high-Ca clinopyroxene compositions include $Mg_{0.84}Ca_{0.72}Fe_{0.34}Si_2O_6$ (Rocknest - sand), $Mg_{0.89}Ca_{0.73}Fe_{0.38}Si_2O_6$ (Gobabeb - sand), and $Mg_{1.03}Ca_{0.75}Fe_{0.21}Si_2O_6$ (Windjana – drilled sandstone); the X-ray refinement method did not allow determination of an aluminous component (Morrison et al., 2018). Expressed in the same terms, the high-Ca clinopyroxene from BCB has an average formula $Mg_{0.93}Ca_{0.77}Fe_{0.27}Al_{0.12}Si_{1.84}O_6$. At least in terms of divalent cation components, it is clear that BCB clinopyroxenes have a similar composition to those

analyzed from Gale crater. The olivine compositions from the same three sample sites in Gale crater listed above are more Fe-rich (ranging from Fo_{54} to Fo_{68}) than olivine in BCB (Fo_{66-86}). However, there is overlap between the highest-Fe olivine from BCB ($Mg_{1.37}Fe_{0.62}SiO_4$) and the highest-Mg olivine from Windjana, Gale crater ($Mg_{1.35}Fe_{0.65}SiO_4$)(Fig. 5). More Mg-rich olivine may exist in Gale crater, but additional high-resolution analyses are required to better sample the population of Gale olivine forsterite contents. As with olivine, the anorthite content of plagioclase from Gale crater differs slightly from that in the BCB samples. Gale crater plagioclase ranges (for all 13 samples inferred in Morrison et al., 2018) in composition from An_{30} to An_{63} with an average of An_{40}, much more sodic on average than plagioclase in BCB but nevertheless displaying an overlap with the high-Na end of the BCB plagioclase distribution (Fig. 5).

The IR-ATR spectra of the BCB samples look quite different from typical orbitally-based infrared reflectance spectra of Mars, e.g. from the Compact Reconnaissance Imaging Spectrometer for Mars (CRISM) instrument. Yet the similarities in mineral chemistry observed in the BCB rocks to the same respective minerals from Gale crater suggest they should have similar bulk spectral properties, as well. Achilles et al. (2017) provide a plausible explanation for the observed differences in their discussion of the CheMin data in relation to the CRISM spectra of the Bagnold Dunes. Although CRISM detects olivine and high-Ca pyroxene in the dune sands, the spectra are strongly modified by a fine-grained dust signal, as are most Martian orbital data. Hence, the surface analyses made by Curiosity (Achilles et al., 2017) are a more suitable point of comparison to the laboratory infrared spectra for assessment of terrestrial analogue candidates. In this context, the detected minerals, mineral compositions, and relative abundances apparent in our IR-ATR spectra are indeed quite similar to the XRD and modal mineralogy derived from APXS results for Gale crater locations, except for the ubiquitous and enigmatic X-ray amorphous component of the CheMin analyzed Martian samples, which are all either sand, soil or sedimentary rocks (Achilles et al., 2017, 2018).

5.4 Balos cove basalts as a valuable locality for activities related to current and future Mars exploration

Although no terrestrial rock is a perfect match to Mars, sample 09IT01, a basaltic tephra from Etna volcano, is already accepted as a leading Mars analogue material and curated by the ISAR (Bost et al., 2013). It has been proposed as an analogue for Gusev basalts despite its subduction affinity (Bost et al., 2013). However, possible uses of the site where 09IT01 was collected for field-scale studies are quite limited. Although Etna volcano is a remarkable and well-studied site for active volcano studies (e.g., Coltelli et al., 2005), 09IT01 is a small sample of unconsolidated tephra from a volcanically active, hazardous, high-relief location (>2400 m). By comparison, BCB rocks form intact flows, unlimited quantities are available, and the site is suitable for field deployments. Santorini island has easy access from sea (frequent ferries from Piraeus port) and air (less than 30 minutes from the Athens International Airport) with exceptional accommodation facilities. The NASA Planetary Science and Technology Analogue Research Program is already investigating the Santorini area because of the unique anoxic environment in the nearby submarine Koloumbo volcano.

A land-based area of outcrop of basalt with properties as close (or closer) to those of the accepted Martian analogue basalt from Etna offers opportunities not only to scientists with special equipment but also to the students to reach the area and collect samples. Field-portable instruments undergoing tests for flight use can be safely used at Balos Cove for testing or calibration purposes. Afterwards, minerals in BCB showing compositional similarities with the respective martian ones can be extracted from the rock matrix using conventional mineral separation or micro-coring techniques. Textural, compositional and spectral analyses of these samples may contribute to calibration of future spectrometers to be deployed on Mars.

In short, the argument for utility of Balos Cove and its basalt outcrops as a useful Martian analogue does not require a perfect match to Martian compositions (that is unobtainable) or any extraordinary uniqueness among terrestrial basalt localities. It depends on a reasonably close match to some mineralogical and chemical aspects of Martian lavas combined with logistical and practical considerations.

6. Conclusions

The BCB rocks display similarities in various properties (mineral chemistry, whole-rock geochemistry, spectroscopy) to the terrestrial rocks that have been classified as

Martian analogues and also to a subset of the Martian shergottites and basalts analyzed by rovers on the surface of Mars. The Balos cove basalts are a good compositional/mineralogical match with a subset of the olivine-phyric and basaltic shergottites. Abundantly available BCB can therefore be a low-cost source of starting material for experiments in lieu of the priceless and rare olivine-phyric shergottites collected on Earth or material laboriously prepared from synthetic mixes. On the other hand, the limitations of the analogy must be kept in mind. The BCB samples misfit with Mars surface basalts in Fe and Al content, and have differing SiO_2 contents to the Gusev basalts. However, given the wide range of SiO_2 contents of Martian meteorites and surface samples, it is difficult to determine what the SiO_2 content of a general-purpose Mars analogue rock should be.

The Balos cove field site is easily accessible and offers excellent logistics for sampling and possible analogue field studies. Santorini Island is reachable by air and sea service and the southern part of the island has a good and safe road network.

In conclusion, the current dataset obtained from Balos cove basaltic rocks in Santorini exhibits characteristics that support the study of this site as a Martian analogue site. More detailed research is in progress, focusing on both in-situ (trace elements on minerals and glasses), and bulk methods (FTIR on hydrated minerals to characterize the degree of alteration).

Acknowledgements

We thank the constructive comments raised by two anonymous reviewers and the editor Dr. Johnson for his editorial handling. Also, we kindly thank Dr. Scott VanBommel for his great help with the handling of the PDS geosciences node data. We greatly thank Dr. G. Economou from Institute of Geology and Mineral Exploration (Athens, Greece) for access on their SEM and XRD facilities. Also, we thank Dr. C. Anagnostou for his efforts to perform the XRF analyses at the Hellenic Centre for Marine Research (HCMR). We acknowledge Dr. Jesús Martinez-Frias for his kindness to review an early version of the manuscript.

Supplementary information

To make a general comparison of the Martian samples to the large population of analyzed terrestrial basalts, we formed continuous two-dimensional histograms of the

42525 basalt compositions compiled in GEOROC and PETDB databases using the method of kernel density estimation. Terrestrial basalt analyses were sorted into four tectonic categories: continental flood basalts (9399 analyses), ocean island basalts (11784 analyses), mid-ocean ridge basalts (7573 analyses) and convergent margin basalts (13769 analyses). We made plots of the distribution of these data in total alkalis vs. SiO_2, in Al_2O_3 vs. MgO, and in FeO* vs. MgO. A probability surface was constructed by summing two-dimensional gaussians centered on each data point with bandwidth equal to typical analytical uncertainty (0.15 for SiO_2, MgO and FeO*, 0.20 for Al_2O_3 and 0.25 for Na_2O+K_2O). These surfaces are shown and compared to Gusev, Shergottite, and BCB compositions for the three pairs of oxides and the four categories of terrestrial basalts, in contour plots in figure 8 and Supplementary Figures S1-S9.

References

Achilles, C. N., Downs, R. T., Ming, D. W., Rampe, E. B., Morris, R. V., Treiman, A. H., ... & Chipera, S. J. (2017). Mineralogy of an active eolian sediment from the Namib Dune, Gale Crater, Mars. Journal of Geophysical Research: Planets, 122(11), 2344-2361.

Achilles, C. N., Downs, G. W., Downs, R. T., Morris, R. V., Rampe, E. B., Ming, D. W., ... & Yen, A. S. (2018). Amorphous Phase Characterization Through X-Ray Diffraction Profile Modeling: Implications for Amorphous Phases in Gale Crater Rocks and Soils. 49th Lunar and Planetary Science Conference, 2083.

Andújar, J., Scaillet, B., Pichavant, M., & Druitt, T. H. (2015). Differentiation conditions of a basaltic magma from Santorini, and its bearing on the production of andesite in arc settings. Journal of Petrology, 56(4), 765-794.

Balta, J. B., Sanborn, M. E., Udry, A., Wadhwa, M., & McSween, H. Y. (2015). Petrology and trace element geochemistry of Tissint, the newest shergottite fall. *Meteoritics & Planetary Science*, *50*(1), 63-85.

Baziotis, I., Kimura, J. I., Pantazidis, A., Klemme, S., Berndt, J., & Asimow, P. D. (2018). Geophysical source conditions for basaltic lava from Santorini volcano based on geochemical modeling. Lithos, 316, 295-303.

Bell III, J. F., Squyres, S. W., Herkenhoff, K. E., Maki, J. N., Arneson, H. M., Brown, D., ... & Hayes, A. G. (2003). Mars exploration rover Athena panoramic camera (Pancam) investigation. *Journal of Geophysical Research: Planets*, 108(E12).

Bost, N., Westall, F., Ramboz, C., Foucher, F., Pullan, D., Meunier, A., ... & Vago, J. L. (2013). Missions to Mars: characterisation of Mars analogue rocks for the International Space Analogue Rockstore (ISAR). Planetary and Space Science, 82, 113-127.

Bridges, J. C., & Warren, P. H. (2006). The SNC meteorites: basaltic igneous processes on Mars. Journal of the Geological Society, 163(2), 229-251.

Buckman, J., Bankole, S. A., Zihms, S., Lewis, H., Couples, G., & Corbett, P. W. (2017). Quantifying Porosity through Automated Image Collection and Batch Image Processing: Case Study of Three Carbonates and an Aragonite Cemented Sandstone. Geosciences, 7(3), 70.

Coltelli, M., Del Carlo, P., Pompilio, M., & Vezzoli, L. (2005). Explosive eruption of a picrite: The 3930 BP subplinian eruption of Etna volcano (Italy). Geophysical Research Letters, 32(23).

Dreibus, G., & Wanke, H. (1985). Mars, a volatile-rich planet. Meteoritics, 20, 367-381.

Druitt, T. H., Edwards, L., Mellors, R. M., Pyle, D. M., Sparks, R. S. J., Lanphere, M., ... & Barreirio, B. (1999). Santorini volcano. Geological Society Memoir, 19.

First, E., & Hammer, J. (2016). Igneous cooling history of olivine‐phyric shergottite Yamato 980459 constrained by dynamic crystallization experiments. Meteoritics & Planetary Science, 51(7), 1233-1255.

Ferrara, G., Fytikas, M., Giuliani, O., & Marinelli, G. (1980). Age of the formation of the Aegean active volcanic arc. Thera and the Aegean world II, 37, 41.

Gellert, R., Rieder, R., Brückner, J., Clark, B. C., Dreibus, G., Klingelhöfer, G., ... & Zipfel, J. (2006). Alpha Particle X‐ray Spectrometer (APXS): Results from Gusev crater and calibration report. Journal of Geophysical Research: Planets, 111(E2).

Gellert, R., & Clark, B. C. (2015). In situ compositional measurements of rocks and soils with the alpha particle X-ray spectrometer on Nasa's Mars Rovers. Elements, 11(1), 39-44.

Goodrich, C. A. (2002). Olivine- phyric martian basalts: A new type of shergottite. Meteoritics & Planetary Science, 37(S12).

Goodrich, C. A. (2003). Petrogenesis of olivine-phyric shergottites Sayh al Uhaymir 005 and Elephant Moraine A79001 lithology A. Geochimica et Cosmochimica Acta, 67(19), 3735-3772.

Greshake, A., Fritz, J., and Stöffler, D. (2004) Petrology and shock metamorphism of the olivine-phyric shergottite Yamato 980459: Evidence for a two-stage cooling and a singe-stage ejection history. Geochimica et Cosmochimica Acta, 68, 3459–2377

Heiken, G., & McCoy, F. (1984). Caldera development during the Minoan eruption, Thira, Cyclades, Greece. Journal of Geophysical Research: Solid Earth, 89(B10), 8441-8462.

Huijsmans, J. P. P. (1985). Calc-alkaline lavas from the volcanic complex of Santorini, Aegean Sea, Greece: a petrological, geochemical and stratigraphic study

(Doctoral dissertation, Instituut voor Aardwetenschappen Rijksuniversiteit Utrecht).

Huijsmans, J. P., Barton, M., & Salters, V. J. (1988). Geochemistry and evolution of the calc-alkaline volcanic complex of Santorini, Aegean Sea, Greece. Journal of Volcanology and Geothermal Research, 34(3-4), 283-306.

IAEA (2013). Analytical Quality in Nuclear Applications Series No. 31. Certification of Trace Element Mass Fractions in IAEA-458 Marine Sediment Sample. IAEA/AQ/31, Austria, 33p.

Karageorgis, A. P., Anagnostou, C. L., & Kaberi, H. (2005). Geochemistry and mineralogy of the NW Aegean Sea surface sediments: implications for river runoff and anthropogenic impact. Applied Geochemistry, 20(1), 69–88. doi:10.1016/j.apgeochem.2004.07.008.

Kemurjian, A. L., Gromov, V. V., Kazhukalo, I. F., Malenkov, M. I., Mishkinyuk, V. K., Petriga, V. N., & Rosentsweig, I. I. (1993). Planet Rovers. Mashinostroyeniye, Moscow.

Marlow, J. J., Martins, Z., & Sephton, M. A. (2008). Mars on Earth: soil analogues for future Mars missions. Astronomy & Geophysics, 49(2), 2-20.

Lafuente, B., Downs, R. T., Yang, H., & Stone, N. (2015). Highlights in mineralogical crystallography. W. De Gruyter, Berlin, 1-30.

McSween, H.Y., Arvidson, R.E., Bell, J.F., Blaney, D., Cabrol, N.A., Christensen, P.R., Clark, B.C., Crisp, J.A., Crumpler, L.S., Des Marais, D.J., and others. (2004). Basaltic rocks analyzed by the Spirit rover in Gusev Crater. Science, 305, 842–845.

McSween, H.Y., Waytt, M.B., Gellert, R., Bell, J.F., Morris, R.V., Herkenhoff, K.E., Crumpler, L.S., Milam, K.A., Stockstill, K.R., Tornabene, L.L., and others. (2006a). Characterization and petrologic interpretation of olivine-rich basalts at Gusev crater, Mars. Journal of Geophysical Research, 111, E02S10.

McSween, H.Y., Ruff, S., Morris, R., Bell, J.F., Herkenhoff, K., Gellert, R., Stockstill, K., Tornabene, L., Squyres, S.W., Crisp, J., and others. (2006b). Alkaline volcanic rocks from the Columbia Hills, Gusev crater, Mars. Journal of Geophysical Research, 111, E09S91.

McSween, H.Y., Ruff, S.W., Morris, R.V., Gellert, R., Klingelhöfer, G., Christensen, P.R., McCoy, T.J., Ghosh, A., Moersch, J.M., Cohen, B.A., and others. (2008). Mineralogy of volcanic rocks in Gusev crater, Mars: Reconciling Mössbauer, alpha

particle X-ray spectrometer, and miniature thermal emission spectrometer spectra. Journal of Geophysical Research, 113, E06S04.

McSween Jr, H. Y. (2015). Petrology on Mars. American Mineralogist, 100(11-12), 2380-2395.

Ming, D. W., Mittlefehldt, D. W., Morris, R. V., Golden, D. C., Gellert, R., Yen, A., ... & Arvidson, R. E. (2006). Geochemical and mineralogical indicators for aqueous processes in the Columbia Hills of Gusev crater, Mars. Journal of Geophysical Research: Planets, 111(E2).

Ming, D. W., Gellert, R., Morris, R. V., Arvidson, R. E., Brueckner, J., Clark, B. C., ... & Klingelhoefer, G. (2008). Geochemical properties of rocks and soils in Gusev crater, Mars: Results of the Alpha Particle X‐ray Spectrometer from Cumberland Ridge to Home Plate. Journal of Geophysical Research: Planets, 113(E12).

Moroz, V. I. (1978). Physics of planet Mars, by Moroz, VI. Moskva (USSR): Nauka, Glavnaya Redaktsiya Fiziko-Matematicheskoj Literatury.

Morris, R. V., D. C. Golden, J. F. Bell, III, T. D. Shelfer, A. C. Scheinost, N. W. Hinman, G. Furniss, S. A. Mertzman, J. L. Bishop, D. W. Ming, C. C. Allen, and D. T. Britt. (2000). Mineralogy, composition, and alteration of Mars Pathfinder rocks and soils: Evidence from multispectral, elemental, and magnetic data on terrestrial analogue, SNC meteorite, and Pathfinder samples Journal of Geophysical Research-Planets, 105, 1757-1817.

Morris, R. V., Klingelhoefer, G., Bernhardt, B., Schröder, C., Rodionov, D. S., De Souza, P. A., ... & Kankeleit, E. (2004). Mineralogy at Gusev Crater from the Mössbauer spectrometer on the Spirit Rover. Science, 305(5685), 833-836.

Morrison, S. M., Downs, R. T., Blake, D. F., Vaniman, D. T., Ming, D. W., Hazen, R. M., ... & Rampe, E. B. (2018). Crystal chemistry of martian minerals from Bradbury Landing through Naukluft Plateau, Gale crater, Mars. American Mineralogist: Journal of Earth and Planetary Materials, 103(6), 857-871.

Neukum, G., & Ivanov, B. A. (1994). Crater size distributions and impact probabilities on Earth from lunar, terrestrial-planet, and asteroid cratering data. Hazards due to Comets and Asteroids, 359.

Nicholls, I. (1970). Petrology of Santorini-volcano, Cyclades, Greece. In: Transactions-American Geophysical Union, Vol. 51 (4), pp. 441.

Nicholls, I. A. (1971). Petrology of Santorini Volcano, Cyclades, Greece. Journal of Petrology, 12(1), 67-119.

Papazachos, B. C., Karakostas, V. G., Papazachos, C. B., & Scordilis, E. M. (2000). The geometry of the Wadati–Benioff zone and lithospheric kinematics in the Hellenic arc. Tectonophysics, 319(4), 275-300.

Papike, J. J., Karner, J. M., Shearer, C. K., & Burger, P. V. (2009). Silicate mineralogy of martian meteorites. Geochimica et Cosmochimica Acta, 73(24), 7443-7485.

Parks, M. M., Biggs, J., England, P., Mather, T. A., Nomikou, P., Palamartchouk, K., ... & Raptakis, C. (2012). Evolution of Santorini Volcano dominated by episodic and rapid fluxes of melt from depth. Nature Geoscience, 5(10), 749.

Reck, H. (1936). Die Geologie der Ring-Inseln und der Kaldera von Santorini. Bd. I–III. Berlin.

Rieder, R., H. Wa¨nke, T. Economou, and A. Turkevich (1997), Determination of the chemical composition of Martian soil and rocks: The alpha proton X-ray spectrometer, J. Geophys. Res., 102(E2), 4027–4044.

Rieder, R., R. Gellert, R. C. Anderson, J. Brückner, B. C. Clark, G. Dreibus, T. Economou, G. Klingelhöfer, G. W. Lugmair, D. W. Ming, S. W. Squyres, C. d'Uston, H. Wänke, A. Yen, and J. Zipfel. 2004. Chemistry of Rocks and Soils at Meridiani Planum from the Alpha Particle X-ray Spectrometer. Science, 306: 1746-1749.

Rubin, A.E., Warren, P.H., Greenwood, J.P., Verish, R.S., Leshin, L.A., Hervig, R.L., Clayton, R.N., and Mayeda, T.K. (2000). Petrology of Los Angeles: A new basaltic shergottite find. Geology, 28, 1011–1014.

Schneider, C.A., Rasband, W.S., Eliceiri, K.W. (2012). NIH Image to ImageJ: 25 years of image analysis. Nature Methods, 9, 671-675.

Snook, K. J., & Mendell, W. W. (2004). The need for analogue missions in scientific human and robotic planetary exploration. In Lunar and Planetary Science Conference (Vol. 35, p. 2130).

Stolper, E., & McSween, H. Y. (1979). Petrology and origin of the shergottite meteorites. Geochimica et Cosmochimica Acta, 43(9), 1475-1498.

Treiman, A. H., Gleason, J. D., & Bogard, D. D. (2000). The SNC meteorites are from Mars. Planetary and Space Science, 48(12-14), 1213-1230.

VanBommel, S. J., Gellert, R., Boyd, N. I., & Hanania, J. U. (2019). Empirical simulations for further characterization of the Mars Science Laboratory Alpha Particle X-ray Spectrometer: An introduction to the ACES program. Nuclear Instruments and Methods in Physics Research Section B: Beam Interactions with Materials and Atoms, 441, 79-87.

Zipfel, J., Schroeder, C., Jolliff, B. L., Gellert, R., Herkenhoff, K. E., Rieder, R., ... & Clark, B. C. (2011). Bounce Rock—A shergottite- like basalt encountered at Meridiani Planum, Mars. Meteoritics & Planetary Science, 46(1), 1-20.

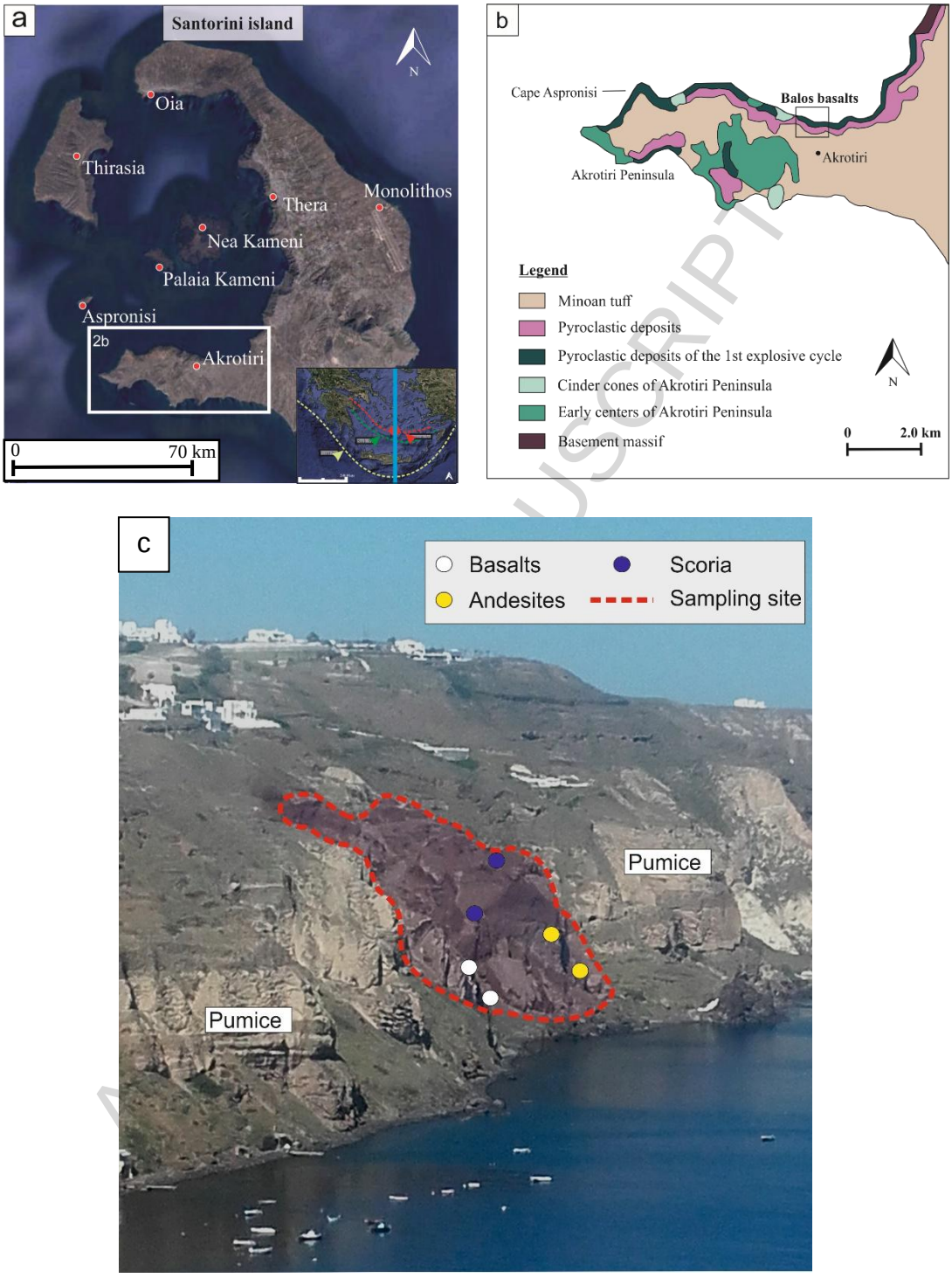

Figure 1. (a) Santorini volcano complex (source: google earth). The white rectangular shows the Akrotiri Peninsula Region (APR). (b) Enlarged simplified geological map of APR showing the sampling region, Balos cove. (c) Field area with sampling sites.

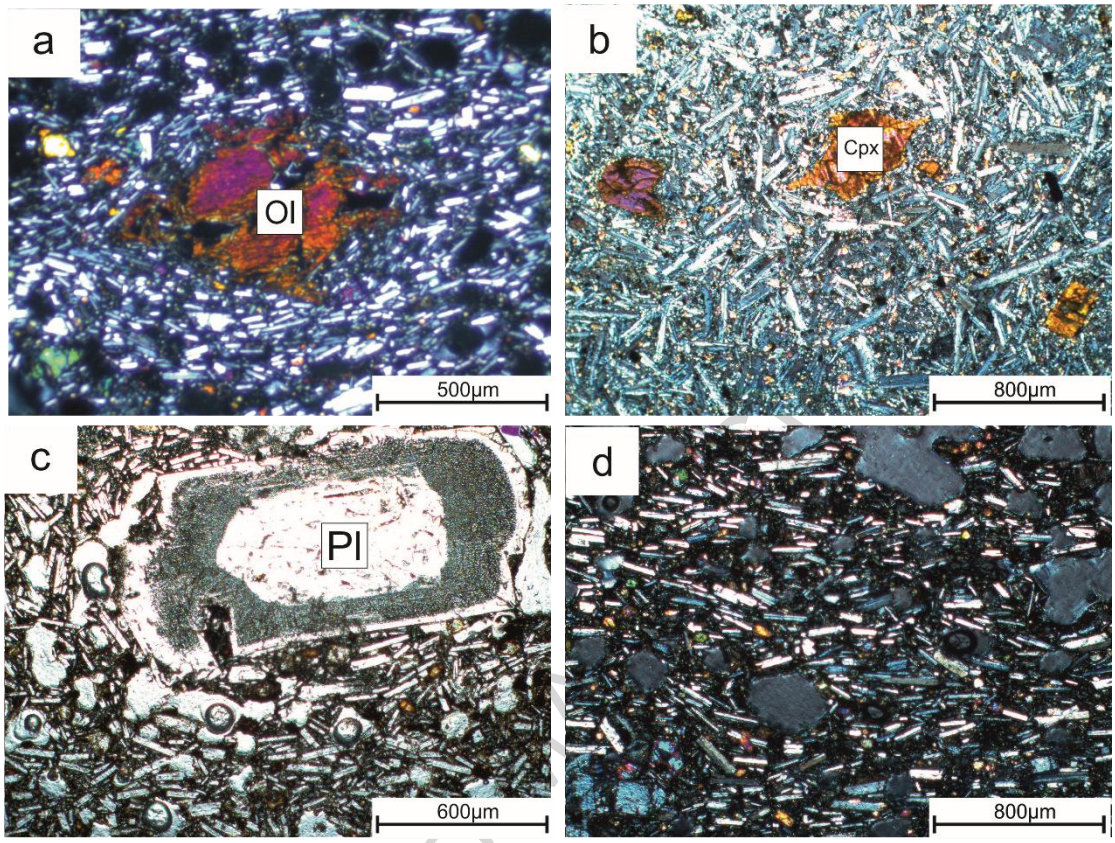

Figure 2. Optical microscope images from Balos cove basalts. a) Subhedral olivine phenocrysts, in a groundmass consisting of olivine macrocryst surrounded by plagioclase crystals. The plagioclase shows a preferred orientation, most likely matching the movement of the lava flow, (b) Clinopyroxene subhedral phenocrysts surrounded by randomly oriented plagioclase microphenocrysts,. (c) A plagioclase megacrysts (~600 µm in diameter) displaying a clear inner core, dark grey intermediate zone, and rimmed by a clear outer zone. d) The groundmass consist of oriented plagioclase microcrysts (up to ~70 µm in length), olivine, pyroxene and devitrified glass.

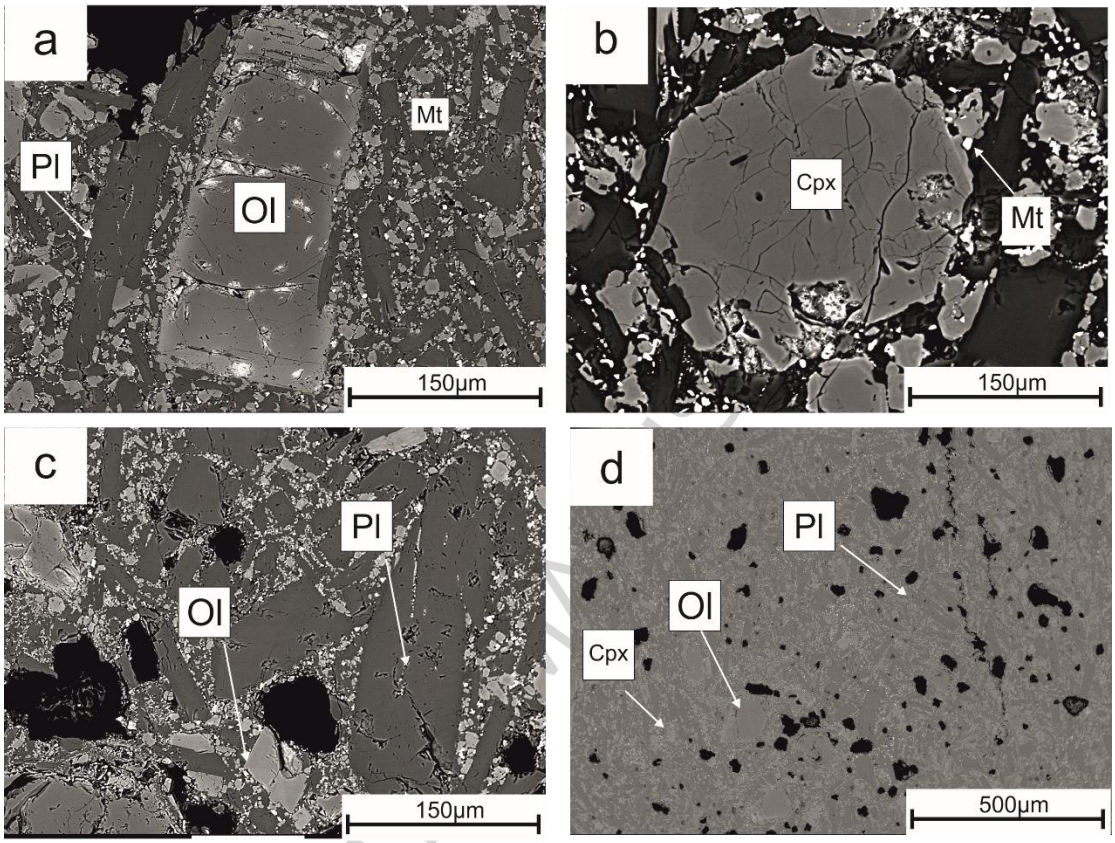

Figure 3. EPMA backscattered images a) Prismatic olivine phenocryst in a groundmass mostly composed by plagioclase. b) Clinopyroxene subhedral phenocryst c) Prismatic crystals of plagioclase. d) Groundmass which consist of prismatic crystals of plagioclase microprismatic crystals of olivine and clinopyroxene.

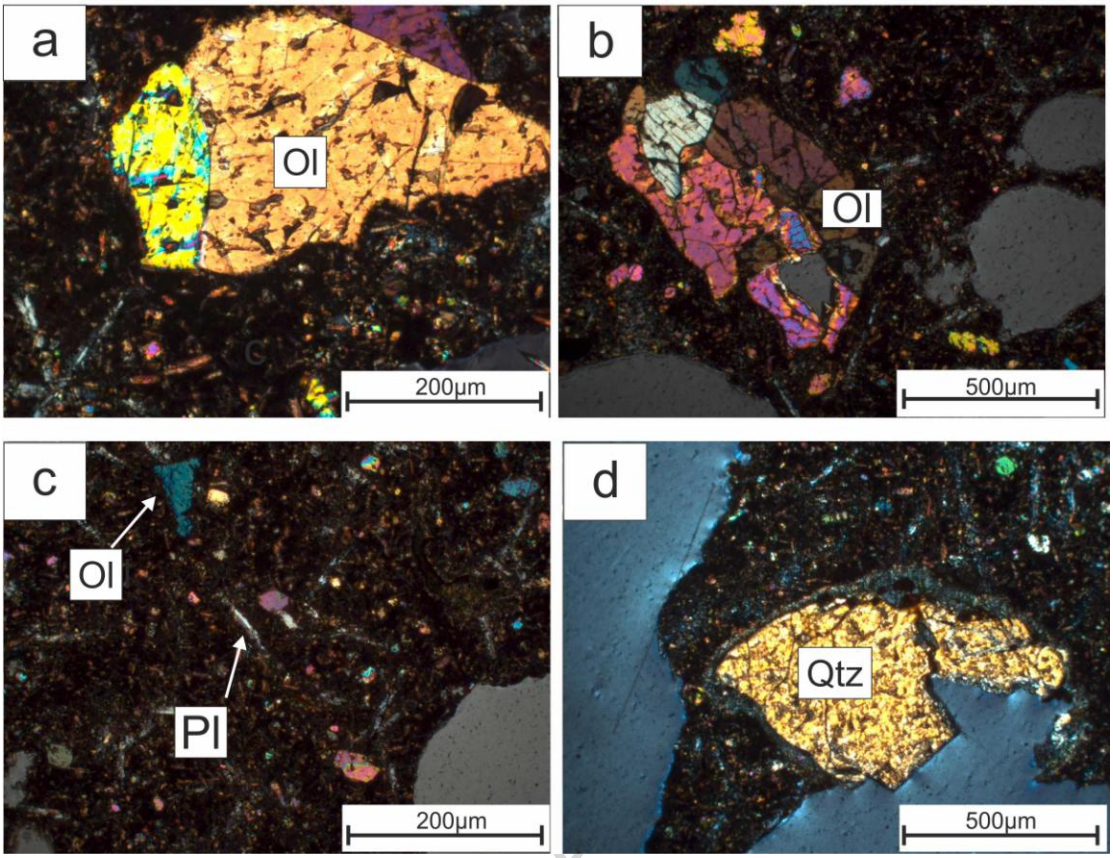

Figure 4. Optical microscope images from ISAR 09SJ15. (a, b) Olivine subhedral phenocryst surrounded by randomly oriented plagioclase in a glassy groundmass. (c) The groundmass consists of randomly oriented plagioclase and microphenocrysts of olivine and pyroxene. (d) A rare quartz xenocryst with anhedral shape.

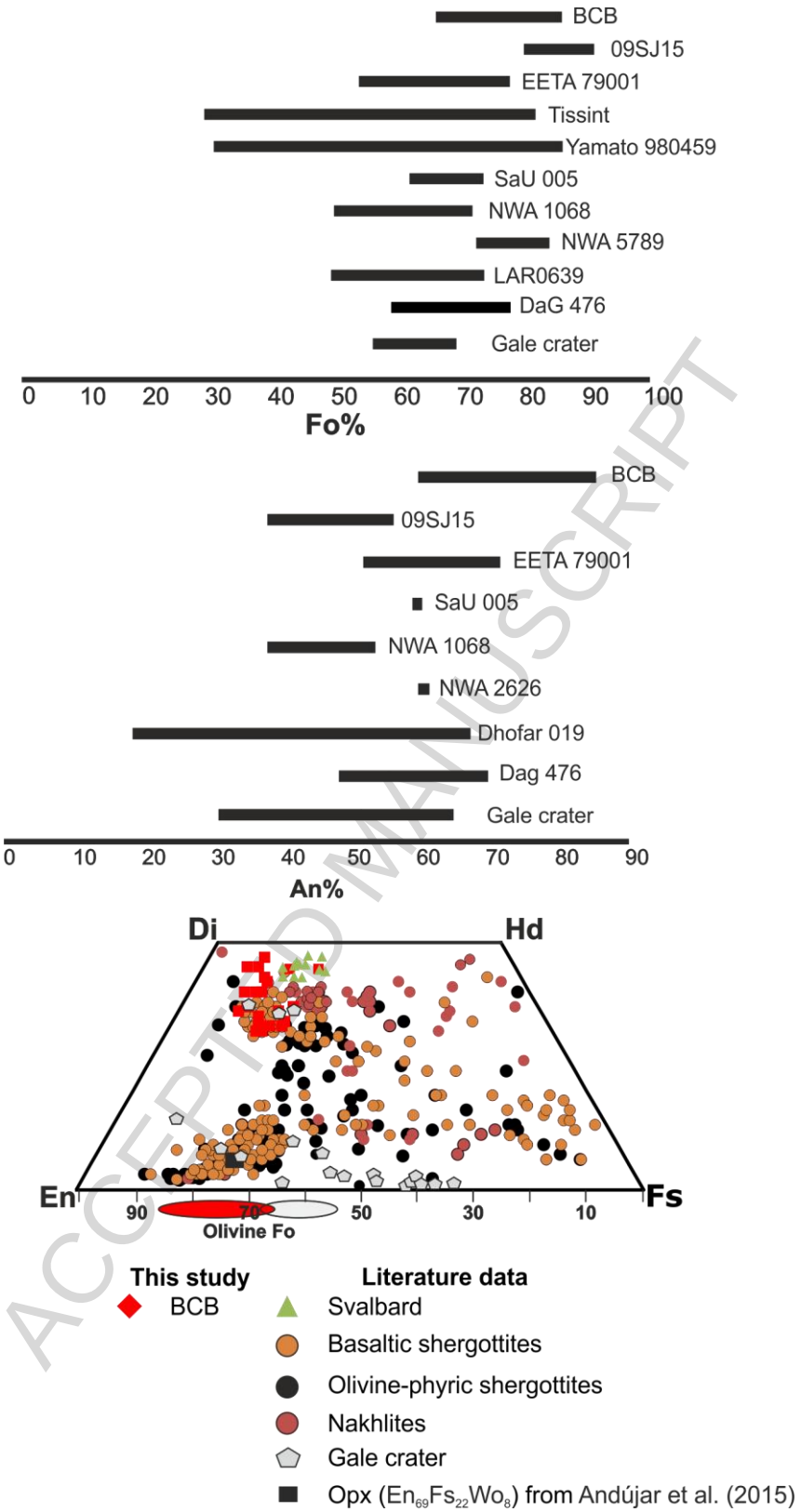

Figure 5. Chemical compositions of olivine (upper part), plagioclase (middle part) and pyroxene (lower part) from BCB, ISAR, Martian shergottites and Gale crater (Morrison et al., 2018). The range of the olivine composition of BCB and Gale crater rocks is given (as ellipses) for comparison below in a pyroxene quadrilateral plot.

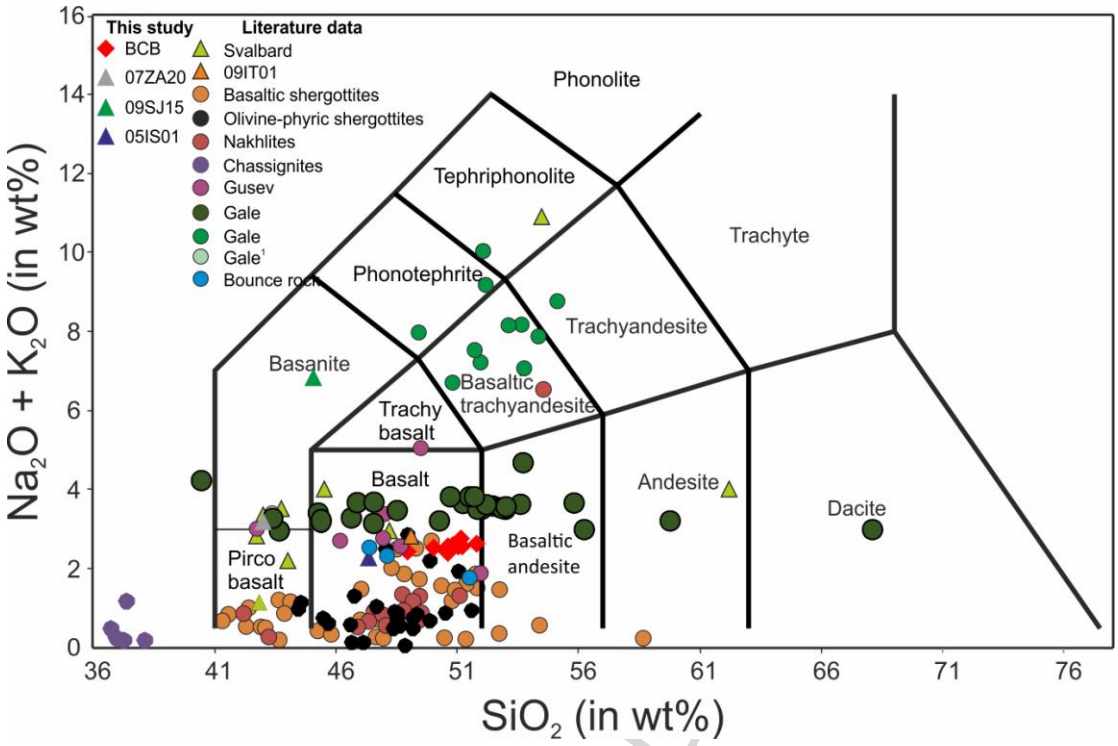

Figure 6. TAS diagram comparing the data from the current study (BCB, ISAR-07ZA20-1, 05IS01), with the published one [ISAR-09IT01 from Bost et al., 2013; Martian meteorites; Svalbard; Gusev and Gale crater (light green and intermediate green) data from Ming et al., 2008 and McSween, 2015)]; Bounce Rock obtained by the Opportunity rover at Meridiani Planum from Zipfel et al. (2011); 1: average basaltic soil in Gale crater from O'Connell-Cooper et al. (2017). The dark green circle correspond to more recent Gale Crater APXS compositional data (Gellert & Clark, 2015; Gellert et al., 2006) which were provided by the PDS Geosciences Node (http://pds-geosciences.wustl.edu/). The data have been filtered (using gnorm>75; svtavg<-30; lifetime>2:00:00; sol range from 150 to 1287) to include only brushed targets interrogated under ideal spectroscopic conditions (e.g., VanBommel et al. 2019). The filtered data are given in supplementary file.

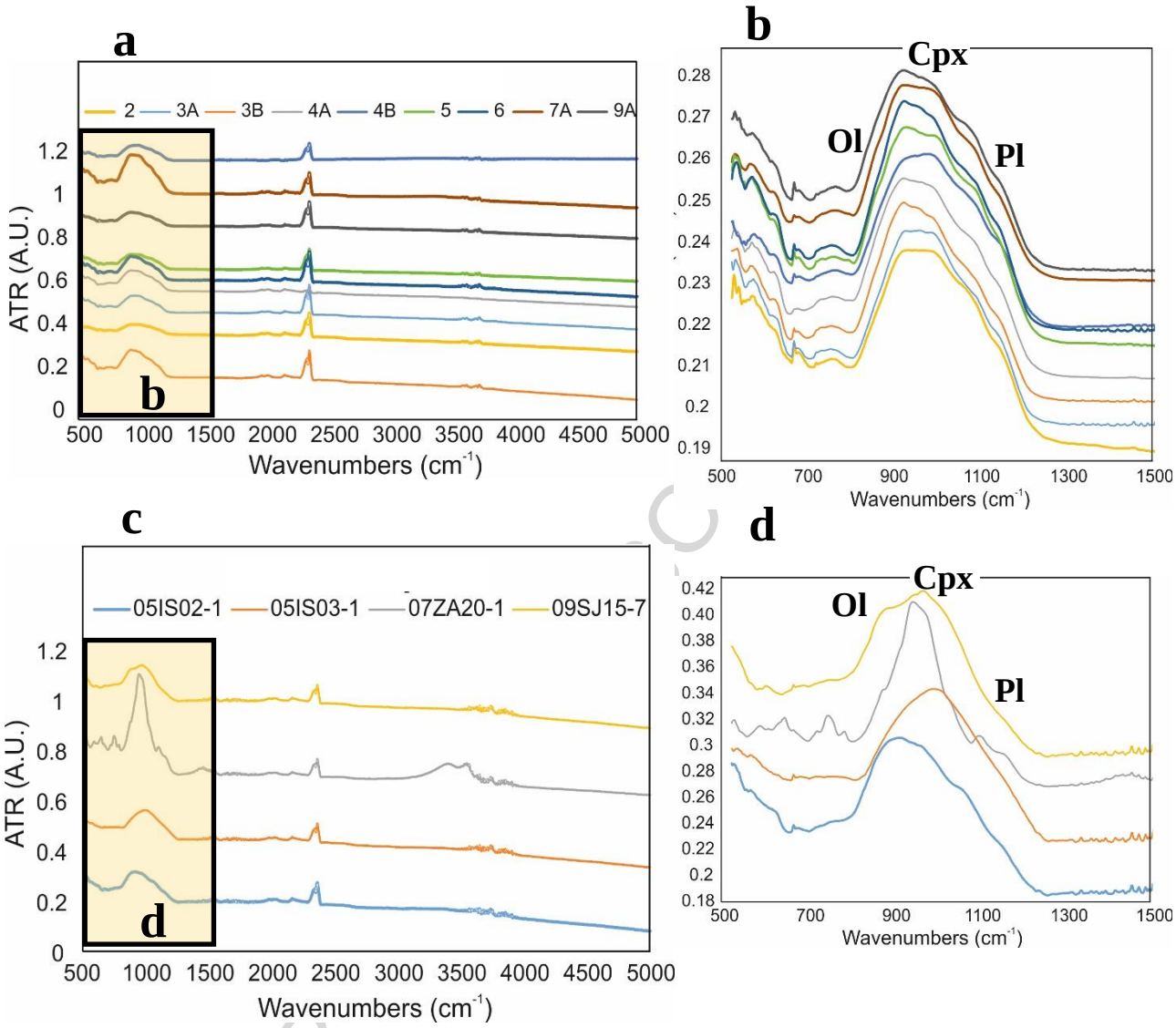

Figure 7. FTIR-ATR patterns for (a,b) BCB and (c,d) ISAR samples. For simplicity, the BCB samples are named excluding the abbreviation "Bal-" but only their number.

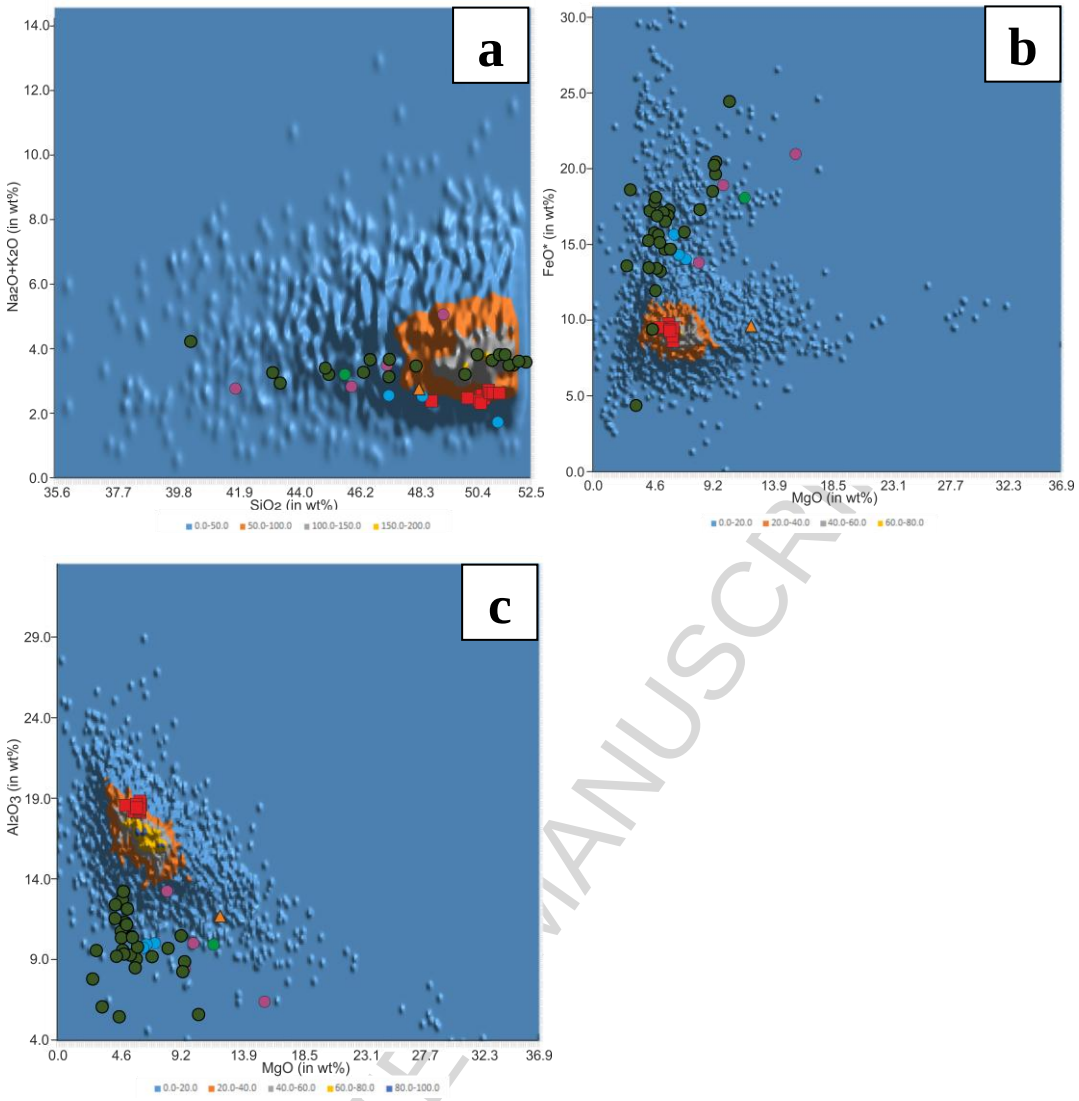

Figure 8. Two-dimensional density plots for convergent margin basalts showing flat contour for (a) SiO_2 vs. Na_2O+K_2O, (b) MgO vs. FeO* and (c) MgO vs. Al_2O_3. The raw data of the terrestrial basalts (~42525 analyses) from the various tectonic settings have been extracted from GEOROC and PetDB databases (http://georoc.mpch-mainz.gwdg.de/georoc/). The BCB (red boxes), ISAR-09IT01 (orang triangle) and Martian surface data (purple circles for Adirondack, Backstay, Irvine and Algonquin; light blue from Bounce rock; light green from Wishstone; dark green from Gale crater as in figure 6) from Gusev crater (Ming et al. 2006, 2008; Zipfel et al. 2011) are superposed for comparison. The details of the plot construction are given in the supplement.

Table 1: Mineralogical properties (X-ray diffraction), and sampling locations of Balos cove basalt samples and samples obtained from the International Space Analogue Rockstore (ISAR) used in this study.

Sample	Nomenclature	Location	Analogue	Ol	Pl	Cpx	Opx^{++}	Qtz	Chl	Amph	Ill
Balos cove basalts											
Bal-2	Basalt	Balos cove	This study	+	+	+					
Bal-3	Basalt	Balos cove	This study	+	+	+					
Bal-4A	Basalt	Balos cove	This study	+	+	+					
Bal-4B	Basalt	Balos cove	This study	+	+	+					
Bal-5	Basaltic andesite	Balos cove	This study	+	+	+					
Bal-6	Basalt	Balos cove	This study	+	+	+					
Bal-7	Basalt	Balos cove	This study	+	+	+					
Bal-8	Basalt	Balos cove	This study	+	+						
Bal-9	Basalt	Balos cove	This study	+	+	+					
International Space Analogue Rockstore Samples											
05IS01	Basalt	Elborgir, Iceland	1	*	*	*					
05IS02	Basaltic sand	Elborgir, Iceland	2	+	+	+		+			
05IS03	Basaltic sand	Hekla, Iceland	2		+	+					
09SJ15	Picritic basalt	Svalbard, Norway	3	+	+	+					+
07ZA20	Altered basalt	Barberton, South Africa	4			+		+	+	+	

+: minerals defined by XRD method; ++: observed in BCB by Andújar et al. (2015); *: minerals defined by petrography in the sheet within ISAR database; 1: Mars basalt; 2: Mars basalt, wind weathering; 3: Alkali-rich tephritic Martian basalts (Gusev Basalt);

4: Noachian basalts-hydrothermal activity; 1-4 based on ISAR characterization (Bost et al., 2013). Mineral abbreviations: Ol: olivine; Pl: plagioclase; Cpx: clinopyroxene; Opx: orthopyroxene; Qtz: quartz; Chl: chlorite; Amph: amphibole.

Table 2: Mineral Chemistry of Balos cove basalt Samples

	Mineral											
Sample	**Bal-4A**	**Bal-4A**	**Bal-4B**	**Bal-4A**	**Bal-4B**	**Bal-4A**	**Bal-4A**	**Bal-4B**	**Bal-4B**	**Bal-4A**	**Bal-4A**	**Bal-4A**
Oxides (in wt%)	**Plc**	**Plc**	**Plc**	**Plr**	**Plr**	**Olr**	**Olint**	**Olc**	**Olc**	**Cpx**	**Cpx**	**Cpx**
SiO_2	51.7	50.1	50.3	53.3	50.0	38.0	39.3	40.4	41.4	50.2	52.7	45.3
Al_2O_3	30.5	31.7	31.1	29.5	31.6					4.8	3.01	1.64
FeO						23.5	18.6	12.8	13.6	8.4	11.3	10.1
MgO						37.7	42	46.8	44.9	15.7	17.2	15.7
CaO	15.3	16	16.9	12.7	15.7					21	15.8	27.3
Na_2O	2.5	2.2	1.73	4.53	2.72							
Total	100	100	100	100	100	100	100	100	100	100	100	100
	Oxygens											
Cations	8					4				6		
Si^{4+}	2.35	2.28	2.29	2.41	2.28	1.02	1.00	1.00	1.04	1.846	1.95	1.81
Al^{3+}	1.63	1.70	1.67	1.57	1.70					0.21	0.13	0.08
Fe^{2+}						0.52	0.40	0.27	0.28	0.16	0.05	0.29
Mg^{2+}										0.86	0.95	0.94
Ca^{2+}	0.74	0.78	0.83	0.62	0.77	1.46	1.60	1.73	1.68	0.83	0.62	1.17
Na^{+}	0.22	0.19	0.15	0.40	0.24							
End-member												
An	78	80	84	61	76							
Ab	22	20	16	39	24							
Fo						74	80	86	85			
Fa						26	20	14	15			
En										44	49	38
Wo										42	33	48
Fs										13	18	14

c: core; r:rim; int:intermediate

Table 3: Mineral chemistry for the ISAR sample 09SJ15									
Oxides (in wt%)	**Pl**	**Pl**	**Pl**	**Ol2c**	**Ol2r**	**Ol**	**Cpx**	**Cpx**	**Cpx**
SiO_2	59.6	58.9	57.6	41.9	39.9	39.2	43.1	47.8	44.5
TiO_2						0.31	6.17	2.8	4.3
Al_2O_3	26.6	26.4	27.7				8.3	5.9	7.66
FeO				8.91	15.1	16.9	10.3	7.5	8.64
MgO				49.2	44.9	43.2	9.93	13.8	12.8
CaO	7.6	9.7	10				22.2	22.2	22.1
Na_2O	6.2	5	4.5			0.31			
Total	100	100	100	100	100	100	100	100	100
	Oxygens								
Cations	8			4			6		
Si^{4+}	2.64	2.62	2.57	1.02	1.00	1.00	1.64	1.78	1.61
Ti^{4+}									
Al^{3+}	1.39	1.38	1.46			0.01	0.19	0.08	0.12
Fe^{2+}							0.37	0.23	0.34
Mg^{2+}				0.18	0.32	0.36	0.33	0.21	0.19
Ca^{2+}	0.36	0.46	0.48				0.56	0.77	0.71
Na^{+}	0.53	0.43	0.39	1.78	1.68	1.62	0.90	0.88	0.89
End-member									
Fo				90	84	81			
Fa				10	16	19			
An	40	52	55						
Ab	60	48	45						
En							32	41	38
Wo							50	47	47
Fs							18	13	15
c: core, r:rim									

Table 4: Whole-rock major element analyses from Selected BCB and ISAR Samples and several Mars basaltic rock classes from Gusev crater and Meridiani Planum.

	Sample												
Oxides (wt%)	**Bal-2**	**Bal-3A**	**Bal-3B**	**Bal-4A**	**Bal-4B**	**Bal-5**	**Bal-6**	**Bal-7A**	**Bal-7B**	**Bal-8A**	**Bal-8B**	**Bal-9A**	**Bal-9B**
SiO_2	50.6	50	49.0	51.0	51.2	51.8	50.9	51.1	50.6	50.8	51.0	50.5	50.7
TiO_2	0.82	0.9	0.81	0.85	0.85	0.86	0.81	0.85	0.83	0.84	0.84	0.82	0.83
Al_2O_3	18.1	18.4	18.7	18.1	18.3	18.5	18.3	18.1	18.5	18.1	18.1	18.2	18.0
FeO*	7.95	8.35	7.45	8.04	8.10	8.17	8.05	8.06	7.86	8.07	8.04	7.33	7.95
MnO	0.15	0.15	0.15	0.15	0.15	0.16	0.15	0.15	0.15	0.15	0.15	0.15	0.15
MgO	6.27	5.93	6.12	6.1	6.13	5.89	6.22	5.39	6.24	6.25	6.13	6.35	5.97
CaO	11.1	10.8	10.6	10.8	10.8	10.8	10.9	10.7	10.6	10.7	10.7	10.8	10.7
Na_2O	1.98	2.07	2.06	2.15	2.15	2.14	2.16	2.24	2.14	2.12	2.14	2.04	2.03
K_2O	0.42	0.46	0.37	0.41	0.42	0.48	0.42	0.53	0.41	0.44	0.45	0.41	0.46
P_2O_5	0.09	0.1	0.08	0.1	0.1	0.1	0.09	0.09	0.1	0.1	0.1	0.09	0.1
Total	97.5	97.2	95.3	97.7	98.2	98.9	98.0	97.2	97.4	97.6	97.7	96.7	96.9
	09SJ15	**05IS01**	**07ZA20-1**	**09IT01**[1]	Adirondack[2]	Backstay[3]	Irvine[4]	Algonquin[5]	Wishstone[6]	Bounce Maggie[7]	Bounce Glanz2[7]	Bounce Case[7]	
SiO_2	45.2	47.7	43.0	48.1	45.9	49.4	47.5	41.9	45.8	47.5	48.5	51.6	
TiO_2	2.56	2.07	2.18	1.02	0.58	0.93	1.06	0.58	0.85	0.69	0.83	0.74	
Al_2O_3	14.0	14.4	15.7	11.3	10.6	13.1	8.3	6.4	10.2	10.7	9.7	10.5	
FeO*	10.1	12.6	14.8	9.38	18.7	13.2	19.7	20.9	17.9	14.2	15.5	14.4	
MnO	0.15	0.21	0.26	0.18	0.41	0.25	0.37	0.39	0.18	0.37	0.42	0.40	
MgO	10.2	6.42	5.45	12.1	9.90	8.3	9.5	16.0	12.6	7.7	6.6	6.8	
CaO	8.21	12.1	9.14	12.7	7.90	6.0	5.8	4.0	4.2	9.8	10.9	12.1	
Na_2O	4.57	2.19	2.88	1.82	2.60	4.0	3.0	2.3	2.97	2.2	2.0	1.7	
K_2O	2.08	0.17	0.30	0.95	0.15	1.02	0.60	0.4	0.23	0.3	0.3	0.1	
P_2O_5	0.76	0.23	0.23	0.29	0.63	1.34	0.94	1.04	1.08	0.88	0.99	0.92	
Total	97.8	98.1	93.9	97.8	97.4	97.5	96.8	93.9	96.0	94.3	95.7	99.3	

References: 1: Bost et al. (2013); 2-5: Ming et al. (2008); 6: Ming et al. (2006) 7: Zipfel et al. (2011)

Table 5: Modal mineralogy based on FTIR-ATR for selected BCB and ISAR samples								
	Sample							
Minerals	Bal-3B	Bal-4B	Bal-5	Bal-4A	Bal-6	05IS02	05IS03	09SJ15
Forsterite		+	+		+	+	+	+
Augite	+	+	+	+	+	+	+	+
Plagioclase	+	+	+	+	+	+	+	+
Magnetite	+				+	+	+	+

Supplementary Figure captions

Figure S1. Two-dimensional density plots for continental flood basalts (CFB) showing flat contour for SiO_2 vs. Na_2O+K_2O. The BCB, and Martian surface data are superposed for comparison (see figure 8 and supplementary information for details).

Figure S2. Two-dimensional density plots for continental flood basalts (CFB) showing flat contour for MgO vs. FeO*. The BCB, and Martian surface data are superposed for comparison (see figure 8 and supplementary information for details).

Figure S3. Two-dimensional density plots for continental flood basalts (CFB) showing flat contour for MgO vs. Al_2O_3. The BCB, and Martian surface data are superposed for comparison (see figure 8 and supplementary information for details).

Figure S4. Two-dimensional density plots for mid-ocean ridge basalts (MORB) showing flat contour for SiO_2 vs. Na_2O+K_2O. The BCB, and Martian surface data are superposed for comparison (see figure 8 and supplementary information for details).

Figure S5. Two-dimensional density plots for mid-ocean ridge basalts (MORB) showing flat contour for MgO vs. FeO*. The BCB, and Martian surface data are superposed for comparison (see figure 8 and supplementary information for details).

Figure S6. Two-dimensional density plots for mid-ocean ridge basalts (MORB) showing flat contour for MgO vs. Al_2O_3. The BCB, and Martian surface data are superposed for comparison (see figure 8 and supplementary information for details).

Figure S7. Two-dimensional density plots for ocean island basalts (OIB) showing flat contour for SiO_2 vs. Na_2O+K_2O. The BCB, and Martian surface data are superposed for comparison (see figure 8 and supplementary information for details).

Figure S8. Two-dimensional density plots for ocean island basalts (OIB) showing flat contour for MgO vs. FeO*. The BCB, and Martian surface data are superposed for comparison (see figure 8 and supplementary information for details).

Figure S9. Two-dimensional density plots for ocean island basalts (OIB) showing flat contour for MgO vs. Al_2O_3. The BCB, and Martian surface data are superposed for comparison (see figure 8 and supplementary information for details).

Highlights

-Santorini volcano as a viable terrestrial analogue of Mars

-The BCB rocks are similar to published analyses of typical olivine-phyric shergottites

-The basalts of Santorini are in family with other Mars basalt analogues and surface samples